Murine bubblegum orthologue is a microsomal very long-chain acyl-CoA synthetase

Peter FRAISL, Sonja FORSS-PETTER, Mihaela ZIGMAN and Johannes BERGER[1]

Division of Neuroimmunology, Brain Research Institute, Vienna University Medical School, Spitalgasse 4, 1090 Vienna, Austria

It has been suggested that a gene termed *bubblegum* (*Bgm*), encoding an acyl-CoA synthetase, could be involved in the pathogenesis of the inherited neurodegenerative disorder X-ALD (X-linked adrenoleukodystrophy). The precise function of the ALDP (ALD protein) still remains unclear. Aldp deficiency in mammals and Bgm deficiency in *Drosophila* led to accumulation of VLCFAs (very long-chain fatty acids). As a first step towards studying this interaction in wild-type versus Aldp-deficient mice, we analysed the expression pattern of the murine orthologue of the *Bgm* gene. In contrast with the ubiquitously expressed *Ald* gene, *Bgm* expression is restricted to the tissues that are affected by X-ALD such as brain, testis and adrenals. During mouse brain development, Bgm mRNA was first detected by Northern-blot analysis on embryonic day 18 and increased steadily towards adulthood, whereas the highest level of Ald mRNA was found on embryonic day 12 and decreased gradually during differentiation. Protein fractionation and confocal laser imaging of Bgm–green fluorescent protein fusion proteins revealed a microsomal localization that was different from peroxisomes (where Aldp is detected), endoplasmic reticulum and Golgi. Mouse Bgm showed acyl-CoA synthetase activity towards a VLCFA substrate in addition to LCFAs, and this activity was enriched in the microsomal compartment. Speculating that *Bgm* expression could be regulated by *Ald* deficiency, we compared the abundance of Bgm mRNA in wild-type and *Ald* knockout mice but observed no difference. Although mouse Bgm is capable of activating VLCFA, we conclude that a direct interaction between the mouse Bgm and the Aldp seems unlikely.

Key words: ABCD1 (ATP-binding cassette, sub-family D), acyl-CoA synthetase, bubblegum, lipidosin, very long-chain fatty acid, X-linked adrenoleukodystrophy.

INTRODUCTION

X-ALD (X-linked adrenoleukodystrophy) is a progressive neurodegenerative disorder inherited via a single gene defect located on the X chromosome [1]. Mutations in the *ABCD1* (*ALD*) gene encoding the ALDP (ALD protein), a peroxisomal half ATP-binding-cassette transporter, result in many phenotypic variants differing in age of onset, symptoms, rate of progression and severity of neurological degeneration [1,2]. Although the precise molecular function of the protein has still not been demonstrated clearly, the binding and hydrolysis of ATP via ALDP has been shown recently [3,4]. The mutated protein causes, in all male patients, an accumulation of straight-chain saturated VLCFAs (very long-chain fatty acids: 22 or more carbons) in their plasma and tissues [1]. Clinically, X-ALD affects mainly the cerebral white matter, spinal cord, peripheral nerves, adrenal cortex and testes [1], although the *ALD* gene is widely expressed among various tissues. This observation has led to the hypothesis that a secondary factor mediates the function of ALDP in a tissue-specific manner.

Biochemically, the accumulation of VLCFA is associated with decreased fatty acid degradation as it was demonstrated that [1-^{14}C]lignoceric acid ($C_{24:0}$) cannot be efficiently degraded via peroxisomal β-oxidation in fibroblasts of X-ALD patients, whereas preactivated substrate, [1-^{14}C]lignoceroyl-CoA, undergoes normal β-oxidation [5]. The activation of VLCFA is catalysed by VLCSs (very long-chain acyl-CoA synthetases). An enzyme with VLCS activity was initially isolated from rat liver peroxisomes, and meanwhile a number of VLCS genes have been described from other species [6–8]. All these enzymes have been localized to microsomal compartments within the cell and are capable of activating a variety of fatty acids including VLCFA. So far, all described VLCS enzymes preferentially activate LCFAs and only to a minor extent VLCFAs. Since impaired peroxisomal VLCS activity is the only known enzymic deficiency in X-ALD, we searched for an ACS (acyl-CoA synthetase), which could be functionally related to ALDP in terms of enzymic acitivity towards VLCFA and with a tissue distribution reflecting the affected organs. The first murine VLCS enzyme that we cloned was expressed only in trace amounts in brain [8], the most severely affected tissue in X-ALD. A second *VLCS*-related gene, cloned by sequence homology, was also not expressed in brain [9]. The first enzyme turned out to activate VLCFA [10] and for the second enzyme, activity mainly on bile acids was shown [11].

Interestingly, Min and Benzer [12] reported the characterization of a gene in *Drosophila melanogaster*, which they termed *bubblegum* (*Bgm*), whose recessive mutation led to neurodegeneration. As can be observed in X-ALD, the mutant fly showed increased levels of VLCFA. Analysis of the gene, using the BLAST algorithm to find similarities to other genes, indicated a strong similarity with the ACS family. Recently [13–15], the human and rodent orthologues of the *Drosophila Bgm* gene were cloned and were reported to be expressed mainly in the target tissues of X-ALD, and it was clearly demonstrated that the mammalian Bgm protein is an ACS. The ability to activate VLCFA has been attributed only to the human protein [13]; for the mouse and rat orthologues, no activity on VLCFA has been reported so far [14,15]. Investigations of the subcellular localization of the

Abbreviations used: ACS, acyl-CoA synthetase; Aldp/ALDP, adrenoleukodystrophy protein; EGFP, enhanced green fluorescent protein; ER, endoplasmic reticulum; EST, expressed sequence tag; HRP, horseradish peroxidase; LCFA, long-chain fatty acid; ORF, open reading frame; PDI, protein disulphide isomerase; PTS, peroxisomal targeting signal; RT, reverse transcriptase; uORF, upstream ORF; UTR, untranslated region; VLCFA, very LCFA; VLCS, very long-chain acyl-CoA synthetase; X-ALD, X-linked adrenoleukodystrophy.

[1] To whom correspondence should be addressed (e-mail johannes.berger@univie.ac.at).

human and the rat protein indicated the presence of Bgm mainly in the cytoplasm [13,15].

In the present study, we extend the current knowledge about mouse *Bgm* at the level of genomic organization, computer-predicted and experimental analyses of the protein structure, subcellular distribution and functional analyses, distribution of the Bgm mRNA in adult tissues and during mouse brain development. Since in the *Drosophila Bgm* mutant a role in VLCFA metabolism was demonstrated, we looked for a spatial and temporal correlation between the Bgm synthetase and the Aldp. In addition, the level of Bgm mRNA expression in the brain of wild-type and *Ald* knockout mice was compared.

MATERIALS AND METHODS

Materials

COS-7 cells were obtained from A.T.C.C. DNA sequencing was performed by MWG-Biotech (Ebersberg, Germany). Computational analysis of mouse Bgm was done using the PSORT II program (http://psort.ims.u-tokyo.ac.jp) and transmembrane prediction was obtained using the TopPred program (http://bioweb.pasteur.fr/seqanal/interfaces/toppred.html). Unless otherwise outlined, all PCRs were performed using *Pyrococcus furiosus* polymerase (Promega, Madison, WI, U.S.A.) to minimize amplification errors. Mouse anti-PDI (protein disulphide isomerase) antibody was purchased from StressGen Biotechnologies (Victoria, BC, Canada), anti-human ALDP antibody from Euromedex (Mundolsheim Cedex, France), mouse anti-GRP78 antibody from Transduction Laboratories (Lexington, KY, U.S.A.), goat anti-rabbit HRP (horseradish peroxidase)-conjugated antibody from Bio-Rad (Hercules, CA, U.S.A.), and goat anti-mouse HRP-conjugated antibody from Dako (Glostrup, Denmark). Rabbit anti-EGFP (enhanced green fluorescent protein) antibody was a gift provided by Professor W. Sieghart (Brain Research Institute, Vienna University Medical School, Austria). Ald-deficient mice [16] and wild-type littermates were from our in-house breeding colony. Protein standard was purchased from MBI Fermentas (Vilnius, Lithuania).

Cloning of mouse Bgm cDNA and generation of expression constructs

We searched the dbEST (non-redundant database of GenBank® + EMBL-DDBJ EST Divison; [17]) with the partial human Bgm sequence (KIAA 0631) and identified several murine EST (expressed sequence tag) clones. Two clones from *Mus musculus* strain C57BL/6, MNCb-1139 (accession no. AA111606) and MNCb-6286 (accession no. AU035394), containing an entire ORF (open reading frame), were made available by the Japanese Collection of Research Bioresources (National Institute of Infectious Diseases, Tokyo, Japan). The insert of clone MNCb-6286 was released from the vector pME18S-FL3 (K. Maruyama and S. Sugano, IMAGE consortium; http://image.llnl.gov) by restriction digest with *Eco*RI and *Xba*I and ligated into pCDNA 3.1+ (Invitrogen, Breda, The Netherlands) resulting in pCDNA3.1:Bgm. To remove the 5′-UTR (untranslated region) and to generate a 5′-*Eco*RI restriction site for the construction of fusion proteins, the mouse Bgm ORF was amplified via PCR using primers 550 (5′-AAAGAATTCCAGCAGATGCCACGC-3′) and 551 (5′-GCTCTAGATGACTACTGTTTTTG-3′) from the template pCDNA3.1:Bgm. The resulting fragment was cloned into pCR3.1 (Invitrogen) to generate plasmid pCR3.1:Bgm (p409). To place the mouse Bgm sequence behind the EGFP ORF, the pEGFP-C1 vector (BD Bioscience, Palo Alto, CA, U.S.A.) was modified to obtain the correct ORF resulting in an EGFP–mouse Bgm fusion construct. Therefore pEGFP-C1 was restricted with *Hin*dIII and overlapping ends were refilled using Klenow enzyme and re-ligated, which resulted in an *Nhe*I restriction site. For insertion of the mouse Bgm cDNA, the modified pEGFP-C1 vector was cut with *Eco*RI–*Sma*I. For mouse Bgm fragment isolation, pCR3.1:Bgm was restricted using *Xba*I (which was end-filled to result in a blunt end) and *Eco*RI. The resulting construct is referred to as pEGFP:Bgm. To position the mouse Bgm ORF in front of the EGFP ORF, the pEGFP-N1 vector (BD Bioscience) was used. To generate an in-frame restriction site at the 3′-end of the Bgm ORF a PCR was performed using the primers 609 (5′-CCTCTAGACCCGCGGCTGTTTTTGCT-3′) and 550, and plasmid pCR3.1:Bgm as a template to obtain the entire Bgm ORF carrying a *Sac*II restriction site at its 3′-end. Fragment insertion was achieved via *Eco*RI–*Sac*II restriction of pEGFP-N1; this construct is referred to as pBgm:EGFP. All constructs were fully sequenced. Genomic analysis of the mouse *Bgm* gene was performed *in silico* using the BLAST mouse genomic algorithm available under http://www.ncbi.nlm.nih.gov/genome/seq/MmBlast.html.

Northern-blot analysis

Fresh mouse tissues (C57BL/6 or hybrid strains back-crossed to C57BL/6) were dissected and snap-frozen for the preparation of total cellular RNA. Tissues were homogenized in 5 ml of guanidine isothiocyanate solution using a Polytron PT3100 homogenizer (Kinematica, Littau, Switzerland) and centrifuged for 10 min at 12 000 ***g*** in an SS34 Sorvall rotor. The supernatant and approx. 1.25 g of CsCl was placed on top of a 5.7 M CsCl solution, after centrifugation at 100 000 ***g*** for 24 h at 22 °C in a Beckman Optima Ultracentrifuge (Fullerton, CA, U.S.A.). The pellet was dissolved in diethyl pyrocarbonate-treated double-distilled water and the RNA precipitated using LiCl and ethanol. The resulting pellets were again dissolved in diethyl pyrocarbonate double-distilled water and the yield of RNA determined by photometric measurement. For Northern-blot analysis, 15 μg of total RNA and a size marker (RNA ladder; BRL, Grand Island, NY, U.S.A.) were fractionated on a 1.2 % (w/v) agarose-formaldehyde gel [18] and transferred to Biodyne B membranes (Pall Corporation, Ann Arbor, MI, U.S.A.). As a control for equal loading and transfer, the blot was probed with a probe of the ubiquitously expressed chicken β-actin mRNA. An 837 bp mBgm cDNA fragment (position 1361–2198; accession no. AU035394) was used for detection of the Bgm mRNA, after radioactive labelling by random priming using [α-^{32}P]dCTP (Hartmann Analytic, Braunschweig, Germany). All blots were hybridized using Express Hyb solution (BD Bioscience) at 68 °C overnight and washed to high stringency [68 °C, 0.2 × SSC (30 mM NaCl/3 mM sodium citrate)/0.2 % SDS] before autoradiographic exposure to the Molecular Imager FX System (Bio-Rad). For the developmental analysis and the comparison of Ald-deficient versus wild-type brain, total RNA was isolated and 1–2 μg of polyadenylated RNA, oligo(dT) selected fraction from 100 μg of total RNA samples and a size marker (RNA ladder; BRL) were fractionated on 1.2 % agarose-formaldehyde gels [18] and transferred to the membrane. As a control of equal loading and transfer, the blot was probed with a mouse cDNA [19] of the ubiquitously expressed cyclophilin [20] or β-actin mRNA. The detection of the mouse Bgm transcript was performed as described above.

RT (reverse transcriptase)–PCR analysis

Approx. 2 μg of total cellular RNA (extracted as described above) was reverse-transcribed and PCR-amplified using the PerkinElmer RT–PCR system with oligonucleotides 432 (5′-ACCCCCTCCAAAGAAGATGGC-3′) and 433 (5′-CGGATCTGCAAAGCAGACCTG-3′). The primer combination was selected such that a 345 bp mBgm-specific product was amplified from the cDNA, but intron 9 in the *mouse Bgm* gene (see Figure 2) discriminates products arising from DNA potentially contaminating the RNA extracts. RT–PCR was performed under conditions not allowing quantitative analysis. As a positive control, RT–PCR of a 680 bp size fragment of the ubiquitously expressed glyceraldehyde-3-phosphate dehydrogenase mRNA, using the primers 420 (5′-ACTGGCGTCTTCACCACCAT-3′) and 421 (5′-TCCACCACCCTGTTGCTGTA-3′), was performed on the same RNA preparations.

Western-blot analysis

For Western-blot analysis, 20 μg of pEGFP-N1, pEGFP:Bgm or pBgm:EGFP was transfected into approx. 2×10^6 COS-7 cells at 220 V and 950 μF by electroporation using the Gene Pulser II System (Bio-Rad). Cells were harvested 72 h after transfection, washed twice in 1 × PBS and lysed by addition of RIPA buffer (500 mM NaCl/50 mM Tris/HCl, pH 7.5/0.1 % SDS/0.5 % sodium deoxycholate/1 % Nonidet P40) and protease inhibitors (1 μg/ml each of leupeptin, pepstatin, aprotinin and 1 mM PMSF). Protein contents were measured using the Bradford assay [21] and approx. 15 μg were separated on an 8 % (v/v) polyacrylamide gel, blotted on to nitrocellulose membrane (Schleicher and Schuell, Einbeck, Germany). For immunodetection, the membrane was blocked with 5 % (w/v) dry milk powder in 1 × TBS solution (150 mM NaCl/25 mM Tris/HCl, pH 7.5) for 1 h at room temperature before adding the following specific antibodies: rabbit anti-EGFP antibody (diluted 1:10 000 in blocking solution), mouse anti-GRP78 antibody (diluted 1:250 in blocking solution) or mouse anti-ALDP antibody [diluted 1:1000 in 1 × TBST (150 mM NaCl/25 mM Tris/HCl 0.05 % (v/v) Tween 20, pH 7.5)] at 4 °C overnight, and with goat anti-rabbit-HRP-conjugated antibody (diluted 1:10 000 in 1 × TBS) or goat anti-mouse HRP-conjugated antibody (diluted 1:20 000 in 1 × TBS) for 2 h at room temperature. Turnover of chemoluminescent substrate was detected using the SuperSignal West Pico Chemiluminescent Substrate kit (Pierce, Rockford, IL, U.S.A.) and Kodak Biomax ML film (Kodak-Eastman, Rochester, NY, U.S.A.).

Indirect immunofluorescence microscopy

Following transfection with pEGFP-N1, pEGFP:Bgm or pBgm:EGFP, COS-7 cells were plated on glass coverslips. After 48 h, cells were fixed for 20 min using a 3 % paraformaldehyde solution at room temperature and later permeabilized with 1 % Triton X-100 for 5 min at room temperature. The primary antibodies (anti-PDI antibody; StressGen Biotechnologies), diluted 1:100 in PBS or a 1:500 dilution of an anti-ALDP antibody (Euromedex), were added for 1 h at room temperature. After washing with PBS several times, the cells were incubated with a secondary anti-mouse biotinylated IgG (1:100 dilution in 1 × PBS) and incubated for 1 h at room temperature. For visualization of the antibody complex, a Cy3-labelled streptavidin molecule (Jackson, West Grove, PA, U.S.A.) was used (1:100 in PBS) and incubated for 1 h at room temperature. After washing the coverslips extensively, the cells were examined using a Zeiss confocal microscope.

Subcellular fractionation

For subcellular fractionation, COS-7 cells were transiently transfected with 20 μg of plasmid pEGFP-N1, pBgm:EGFP, pEGFP:Bgm or hs (homo sapiens) ALDP in pCDNA 3.1 (p118) by electroporation at 220 V and 950 μF. Cells were harvested 72 h after electroporation by trypsinization and washed twice with PBS. For ALDP fractionation from HeLa cells, cells were grown to confluency, harvested by trypsinization and washed twice with 1 × PBS. The cell pellets were resuspended in STE buffer (10 mM Tris/HCl, 1 M NaCl/1 mM EDTA, pH 8), supplemented with a mixture of protease inhibitors (see Western-blot analysis section above) and homogenized by 15 strokes of a glass–Teflon Potter–Elvehjem homogenizer. The suspension was centrifuged at 600 ***g*** for 5 min at 4 °C for preparation of a post-nuclear supernatant, which was centrifuged again at 10 300 ***g*** for 10 min at 4 °C to obtain a crude mitochondrial fraction. The remaining supernatant was used for centrifugation at 100 000 ***g*** for 1 h at 4 °C in a Beckman Optima ultracentrifuge to separate microsomes and cytoplasm. Protein content was determined using the BioRad protein assay [21].

Acyl-CoA activity assay

Electroporated cells were harvested 3 days after transfection and subcellular fractions were prepared as described above and stored at − 80 °C before assay. [1-^{14}C]Palmitic acid ($C_{16:0}$), [1-^{14}C]linoleic acid ($C_{18:2n-6}$) and [1-^{14}C]lignoceric acid ($C_{24:0}$) were solubilized by brief sonication and incubation at 37 °C in 10 mM Tris/HCl (pH 8) containing 10 mg/ml α-cyclodextrin. Assay of activation of 1-^{14}C-labelled fatty acids was performed as described elsewhere [22].

RESULTS

Cloning and characterization of the murine Bgm cDNA

To obtain cDNA clones of the murine Bgm orthologue, we screened the GenBank® non-redundant database for EST clones with a high similarity to the human KIAA0631 protein, an incomplete ORF consisting of 634 amino acids, encoded by the human *BG* gene [13]. We identified two murine cDNA clones (MNCb-1139 and MNCb-6286) with 89.4 % nucleotide sequence identity to the human sequence. Both clones contained a complete ORF. These clones were obtained from the Japanese Collection of Research Bioresources GenBank® (Japan) and sequenced entirely, revealing slight differences in sequence composition. Clone MNCb-6286 (accession no. AU035394), whose sequence was identical with the GenBank® entry NM_053178 [14], was chosen for further analysis. The entire cDNA structure, including the 5′- and 3′-UTRs, predicted ORF and protein features are shown in Figure 1(A). Detailed analysis of the 5′-UTR revealed three stop codons at positions − 159, − 140 and − 16 and three additional potential translation initiation codons at positions − 124, − 80 and − 13. The first ATG (− 124) forms an upstream ORF (uORF) with the stop codon at position − 16. uORFs regulate the amount of protein made by minimizing the initiation events at the main start codon (+ 1 ATG) [23–25]. This finding could imply a possible regulatory mechanism at the level of translational initiation for the mouse *Bgm* gene. Topographical analysis of the protein, encoded by the major ORF (721 amino acids), using the TopPred 2

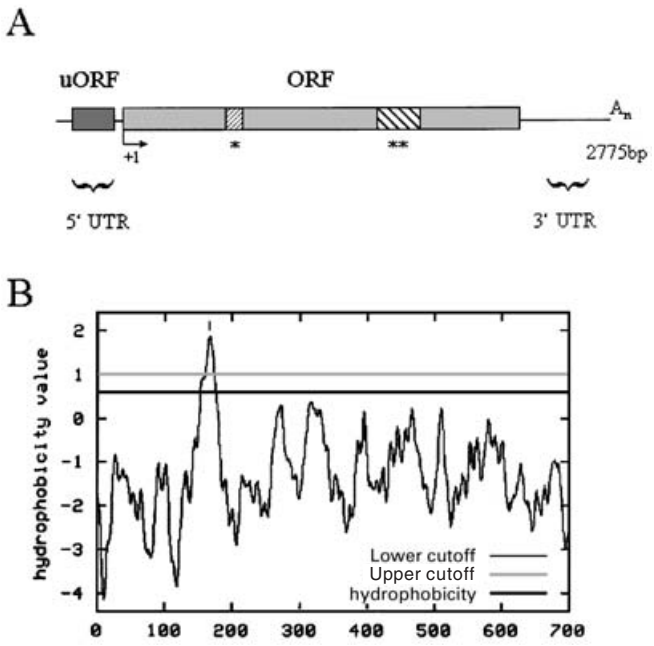

Figure 1 Specific features of the mouse Bgm cDNA and protein

(**A**) Schematic representation of murine Bgm cDNA. Dark grey box marks the uORF, grey box the ORF, including the translation start site indicated by +1. *, AMP-binding domain; **, conserved Bgm motif (by the method of Steinberg et al. [13]). (**B**) Hydrophobicity plot of mouse Bgm protein. Predicted transmembrane sequence of the murine Bgm based on analysis of the amino acid sequence with TopPred. Values > 1 denote hydrophobic regions that tend to be buried inside the molecule or within the hydrophobic membrane environment.

program identified a single membrane-spanning domain in the N-terminal part of the protein starting at position 167 and ending at 187 (Figure 1B). These results could be confirmed by using other transmembrane-predicting programs such as TMpred and HMMTOP (http://www.ch.embnet.org/software/TMPRED_form.html; http://www.enzim.hu/hmmtop). Sequence motifs found in all ACSs (AMP-binding sites) and a motif specific for the Bgm synthetase family [13] are indicated in Figure 1(A). Analysis *in silico* of the genomic structure of mammalian *Bgm* genes (Figure 2) revealed an organization of 14 exons and 13 introns (see the Discussion section for further details). The mouse *Bgm* gene is located on chromosome 9B.

Tissue distribution of mouse Bgm mRNA

The size and tissue distribution of the mouse Bgm mRNA was determined by Northern-blot analysis. A single transcript corresponding to a 2.9 kb mRNA species was detected in brain, testis and adrenals (Figure 3A), but not in skeletal muscle, heart, lung, spleen and kidney. The abundance of the detected transcript was similar for the three tissues when normalized to the β-actin mRNA used as a control for loading and transfer. Using a more sensitive assay, reverse-transcription-coupled PCR (RT–PCR), a strong amplification product indicative of mouse Bgm mRNA expression, was obtained from brain, testis and adrenals and additionally weak amplicons from liver, kidney and lung (results not shown). Although the RT–PCR was not performed in a quantitative manner, only weak bands were obtained in these tissues indicating that the mouse Bgm mRNA is only present in very small amounts here.

Expression profile of mouse Bgm during mouse brain development

To evaluate the possibility of a co-ordinated temporal regulation of the *Ald* and *Bgm* genes during mouse brain differentiation, the developmental time course of mouse Bgm mRNA expression was investigated. By Northern-blot hybridization, the 2.9 kb Bgm

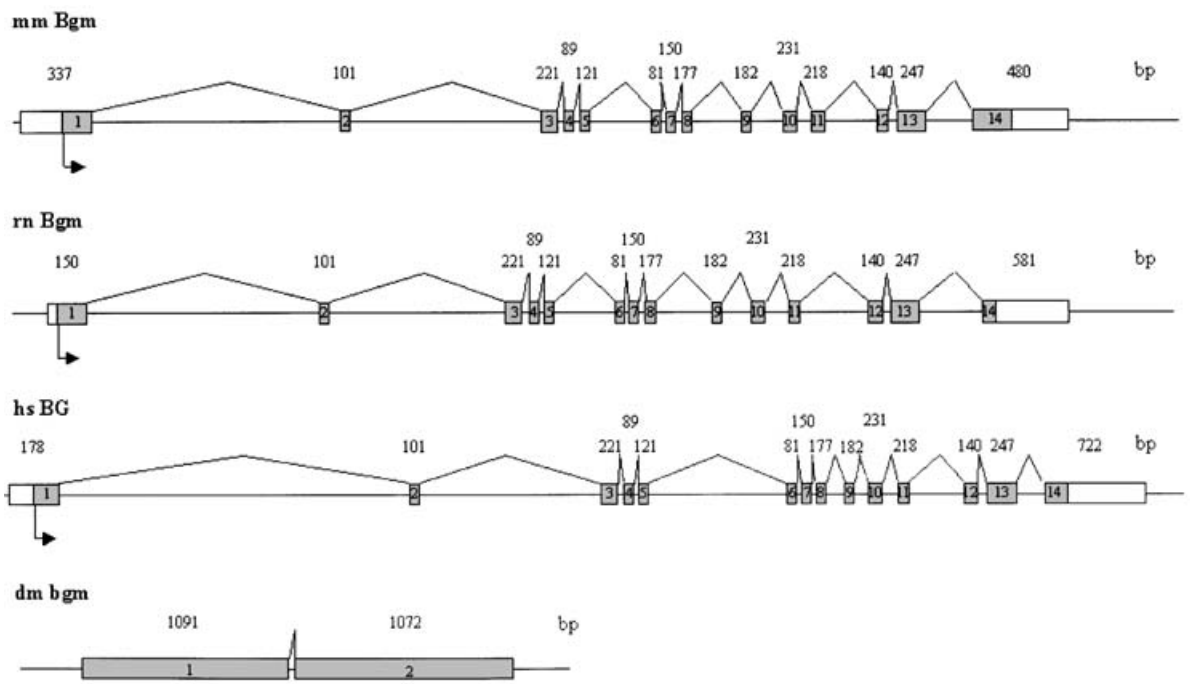

Figure 2 Schematic comparison of the mouse (mm) *Bgm*, rat (rn) *Bgm*, human (hs) *BG* and the *Drosophila* (dm) *Bgm* gene structures

Exons are shown as rectangles with the coding region filled (in grey) and the UTRs being empty. Above each exon its size in bp is indicated. The arrow marks the start of the coding region. The number of exons, beginning with the first identified exon, are indicated within the exon rectangles.

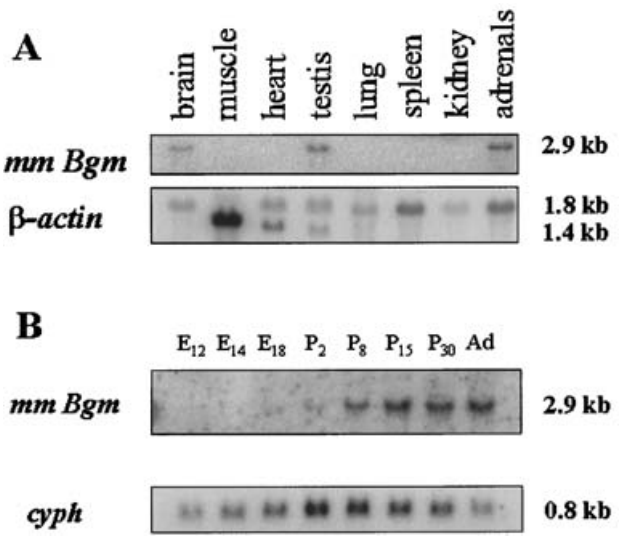

Figure 3 Northern-blot analysis of the mouse Bgm transcript

(**A**) Northern-blot analysis of Bgm mRNA expression in murine (mm) tissues. Total RNA (15 μg), pooled from two male animals, was hybridized with a ^{32}P-labelled mouse Bgm cDNA probe. Approximate sizes of the detected bands are shown on the right. A control hybridization with a β-actin probe is shown in the lower panel. (**B**) Northern-blot analysis of mouse (mm) Bgm mRNA distribution during brain development. Polyadenylated RNA (1–2 μg/lane) was extracted from dissected brain or whole head (lanes E_{12} and E_{14}) at the indicated developmental stages and hybridized with ^{32}P-labelled cDNA probes. Upper panel, mouse Bgm; lower panel, cyclophilin (cyph) as loading control. The approximate sizes of the transcripts are shown on the right. The lanes are labelled as follows: E_{12}–E_{18}, 12.5–18.5 days of gestation; P_2–P_{30}, days of postnatal development; Ad, adult brain.

transcript was first detected in the central nervous system at the late embryonic stage (E_{18}, embryonic day), increasing in constant amount towards adulthood (Figure 3B). Interestingly, the Bgm expression pattern shows a typical post-synaptic neuron-enriched profile. This is in contrast with the Ald mRNA, whose expression is the highest in the immature mouse brain and gradually decreases during differentiation [26].

Expression of mouse Bgm in wild-type and Ald-deficient mouse brain

Based on the observation that the *D. melanogaster* mutant *Bgm* showed accumulation of VLCFA and a neurodegenerative phenotype, suggesting an involvement of Bgm in X-ALD, we examined if the Bgm mRNA level is affected by Ald deficiency in mice. By Northern-blot analysis, the steady-state level of the mouse Bgm mRNA is similar in brain of adult wild-type and Ald knockout mice (Figure 4). This is clearly illustrated when normalizing the signal intensity to the β-actin control for loading and transfer (lower panel). Two different animals of each phenotype were analysed, increasing the significance of this experiment.

Subcellular distribution

A computational analysis of the hypothetical protein, resulting from the mouse *Bgm* gene, with the PSORT II algorithm revealed a putative PTS-2 (peroxisomal targeting signal 2) [27] (KIWKDLPHL), starting at amino acid 218. This position within the protein is not a typical localization of a PTS-2 signal. Furthermore, two potential ER (endoplasmic reticulum) retention signals were predicted by PSORTII: the first is located at the very N-terminus of the protein at position 2 (PRGS) and resembles an

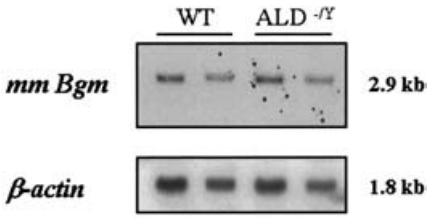

Figure 4 Northern-blot analysis of mouse Bgm mRNA levels in wild-type versus Ald-deficient brain

Polyadenylated RNA (1–2 μg/lane) was extracted from the brain of adult wild-type and Ald knockout mice and hybridized with ^{32}P-labelled cDNA probes. Upper panel, mouse (mm) Bgm; lower panel, β-actin as control for loading and transfer. The approximate sizes of the transcripts are shown on the right.

XXRR-like motif; the second shows similarity with a KKXX-like retention motif at the C-terminus (QEQK) at amino acid position 717. No other targeting signals could be found.

For investigating the subcellular distribution of the mouse Bgm protein, a construct encoding a mouse Bgm–EGFP fusion protein was generated. To rule out the possibility that the fusion of the EGFP protein to the mouse Bgm protein changes its distributional behaviour within the cell, we performed an N-terminal (pEGFP:Bgm) as well as a C-terminal (pBgm:EGFP) EGFP fusion. The specificity and expression of the pEGFP:Bgm and pBgm:EGFP products were assessed by Western-blot analysis of total cellular extracts (results not shown). A single band corresponding to approx. 110 kDa was detected in transfected COS-7 cells for both pEGFP:Bgm and pEGFP:Bgm fusion constructs, whereas a 30 kDa EGFP band was detected only in pEGFP-N1-transfected COS-7 cells, which served as a control for the antibody specificity. To establish the distribution within the cells, COS-7 cells were electroporated with pEGFP:Bgm, pBgm:EGFP or pEGFP-N1 constructs and subcellular fractions were prepared. The quality of the fractions was analysed by Western-blot detection using EGFP as a marker for the cytoplasmic fraction [28], GRP78 as a marker for the ER [29,30] (but see [30a]) and the ALDP as a peroxisomal marker [31]. As can be seen in Figure 5(A, lane 2), most of the EGFP resides in the cytoplasmic fraction. The GRP78 protein could be detected in mitochondrial and microsomal fractions only (Figure 5B, lanes 1, 3, 4, 6, 7, 9), which are the fractions where ER proteins are typically detected [32]. In addition, the ALDP appears only in the microsomal fraction (Figure 5C, lanes 3 and 6), which in this fractionation protocol contains the peroxisomes. This is the case for both transiently transfected ALDP in COS-7 cells and naturally residing ALDP in HeLa cells (Figure 5C, lanes 1–3 and 4–6 respectively). The EGFP antibody detected most of the Bgm fusion proteins in the microsomal fraction (Figure 5A, lanes 6 and 9). Smaller amounts could also be found in the cytoplasmic (Figure 5A, lanes 5 and 8) and in the mitochondrial fractions (Figure 5A, lane 4). Both the N- and C-terminal fusion proteins showed a similar distribution within the mitochondrial, cytoplasmic and microsomal fractions (Figure 5A, lanes 4–9). These results clearly demonstrate that most of the fusion proteins can be found in membrane fractions, which confirms the computational predictions.

Subcellular localization

On the basis of the results that we obtained from the subcellular fractionation experiments, we performed confocal microscopy on our N- and C-terminal EGFP fusion constructs. As the largest

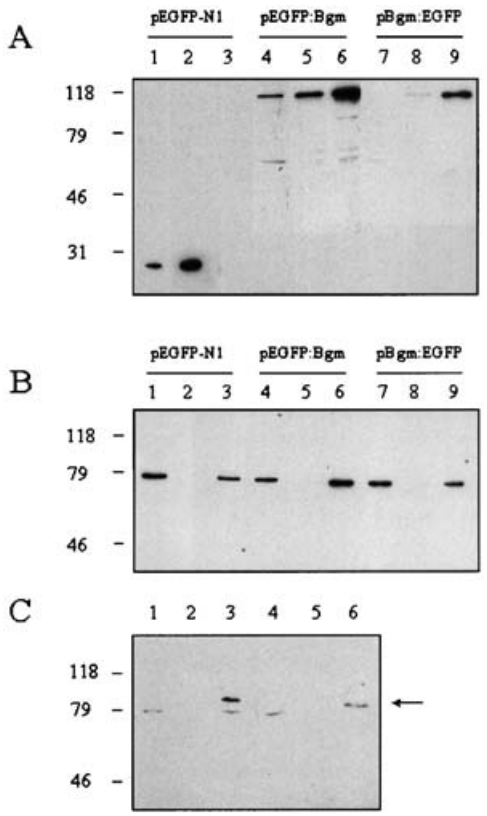

Figure 5 Subcellular fractionation of mouse Bgm–EGFP fusion constructs

(**A**, **B**) COS-7 cells were electroporated with pEGFP-N1 (lanes 1–3), pEGFP:Bgm (lanes 4–6) or pBgm:EGFP (lanes 7–9) and harvested 72 h after transfection. Cells were homogenized and subcellular fractions separated by centrifugation resulting in a mitochondrial fraction (lanes 1, 4 and 7), a cytoplasmic fraction (lanes 2, 5 and 8) and a microsomal fraction (lanes 3, 6 and 9). (**A**) Distribution within the subcellular fractions of the mouse Bgm fusion protein using an anti-EGFP antibody for detection. (**B**) Distribution of the ER marker GRP78. (**C**) HeLa cells were grown to confluence and harvested for detection of endogenous ALDP (lanes 1–3). COS-7 cells were electroporated with p118 (hs ALDP in pCDNA 3.1) and harvested 72 h post-transfection (lanes 4–6). Cells were homogenized and subcellular fractions obtained by centrifugation resulting in a mitochondrial fraction (lanes 1 and 4), a cytoplasmic fraction (lanes 2 and 5) and a microsomal fraction (lanes 3 and 6). Position of the ALDP signal is indicated by an arrow. Masses (kDa) of the protein standards used are indicated on the left-hand side of the blots.

amounts of the proteins could be found in the microsomal fraction (Figure 5A, lanes 6 and 9), we used the ER marker protein disulphide isomerase (PDI) [33] and the peroxisomal membrane protein ALDP for co-localization experiments. As expected for a microsomal localization, the results showed a punctated staining in COS-7 cells (Figures 6a, 6d and 6g) for both Bgm fusion constructs. In addition, we observed a slight background signal throughout the cell (Figures 6a, 6d and 6g), which could be due to the presence of some fusion molecules in the cytoplasmic compartment (Figure 5A, lanes 5 and 8), probably due to the hydrophilic properties of the EGFP domain within the fusion proteins or to the level of overexpression. However, the ER marker (Figures 6c and 6f) showed no significant co-localization, which would have been seen as a yellow colouring in the overlay view. Also the ALDP protein, which is situated in the peroxisomal membrane, revealed no significant co-localization with the Bgm–EGFP fusion protein, although occasional signals seemed to overlap (Figures 6h and 6i). Also immunofluorescence using an anti-Golgi marker (GM130) showed no co-localization (results not shown). These results indicate that our Bgm fusion proteins reside in a microsomal compartment, other than the ER, Golgi or peroxisomes.

ACS activity

The various fractions containing the fusion protein pEGFP:Bgm (Figure 5, lanes 4–6) were assayed for ACS acitivity. As shown in Table 1, only the microsomal fraction showed significant activity towards palmitic acid ($C_{16:0}$) and lignoceric acid ($C_{24:0}$). Mitochondrial and cytoplasmic fractions showed no significant activation of palmitic acid and lignoceric acid, but showed a significant activity towards linoleic acid ($C_{18:2n-6}$). The amount of ACS activity was generally lower in the cytoplasmic fraction when compared with the microsomal fraction. The mitochondrial fraction showed intermediate levels. However, comparison of numeric values is not possible because these results were obtained from independent experiments. Basically, the Bgm-expressing fractions showed much more activity for the two LCFAs (long-chain fatty acids) than for VLCFA. As the results from the pEGFP-N1-transfected controls illustrate and as expected [34–36], most of the ACS activity is located in microsomes. Similar results were obtained when analysing the native mouse Bgm protein expressed under the same conditions as the fusion proteins (results not shown). These results show that mouse Bgm is capable of activating VLCFA but exhibits higher activity for LCFA.

DISCUSSION

In the present study, we have investigated the mouse orthologue of the *D. melanogaster* gene *Bgm*, also termed *lipidosin* [14]. For this purpose, we searched the databases for murine Bgm candidates and obtained a suitable cDNA clone containing an entire ORF, which gives rise to a deduced protein sequence of 721 amino acids. This protein contains several features characteristic for an ACS [37,38], such as an AMP-binding domain and a motif conserved within the Bgm family, which exhibits slight similarities to known VLCS motifs [13]. Homology comparisons of the primary amino acid sequence resulted in 92 % similarity to the human BG protein and 99 % to the rat orthologue but only 61 % similarity to *D. melanogaster* Bgm. Recently, these cDNAs have been cloned and characterized [12,13,15]. The *Drosophila Bgm* gene was identified in a screen for mutations leading to severe neurodegeneration. This observation turned out to be of particular interest in the context of X-ALD as the mutant flies showed increased levels of VLCFA [12]. To explore a possible structural and functional relationship between the mammalian genes, we analysed the genomic organization of human, mouse and rat genes (Figure 2). The three genes seem to have a common origin since the genomic organization shares several features: all three genes consist of 14 exons, 13 introns and similar exon/intron boundaries, and show similarities in exon lengths and exon cluster formation. In contrast, the *Drosophila* gene consists of only two exons, separated by a small intron. Yet another Bgm orthologue has been described for the insect *Anopheles gambiae* (accession no. EAA10184), with a completely different organization of the gene (http://www.ncbi.nlm.nih.gov/LocusLink). This could imply a different origin of the genes from insects and mammals. Nevertheless, the resulting proteins might be functionally comparable, which we think is the case for the mammalian Bgm family.

Functional analyses of our EGFP:Bgm and Bgm:EGFP fusion proteins clearly show that most of the proteins reside in the microsomal fraction with smaller amounts of the proteins detectable in the cytosolic and mitochondrial fractions, whereas most of the EGFP protein, which serves as a control, could be found

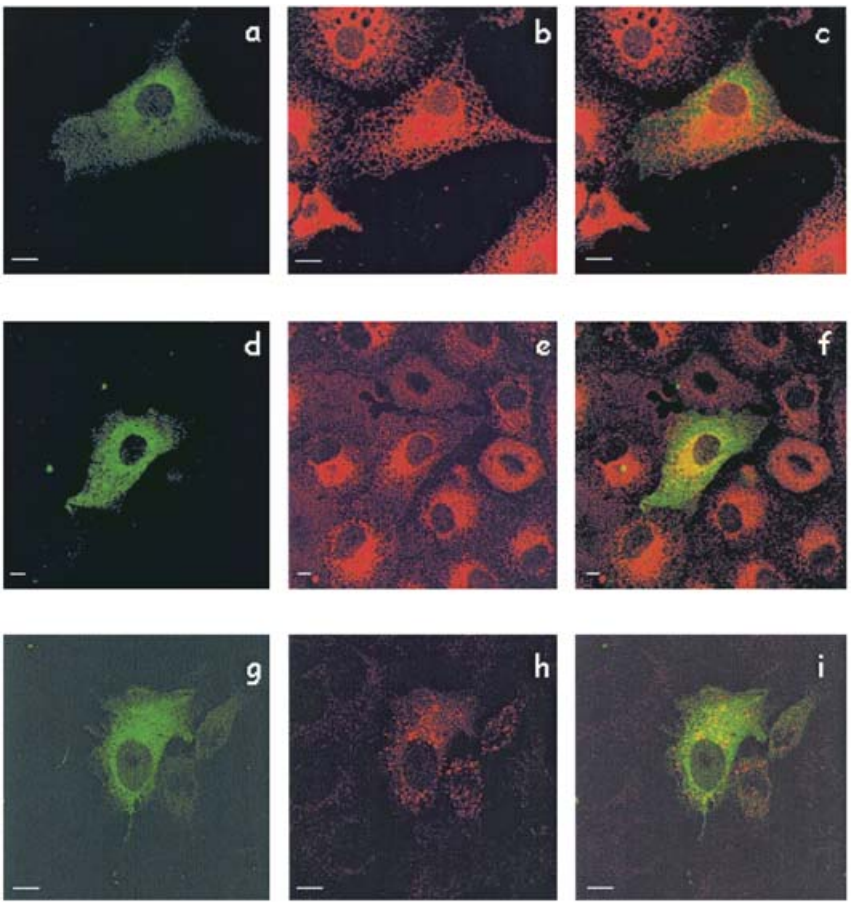

Figure 6 Subcellular localization of mouse Bgm in transfected COS-7 cells by confocal microscopy

For confocal analysis of the Bgm–EGFP fusion constructs, pEGFP:Bgm or pBgm:EGFP alone (**a**–**f**) or together with human (hs) ALDP (**g**–**i**) were transfected into COS-7 cells, fixed and permeabilized and then incubated with mouse anti-PDI or mouse anti-ALDP antibodies. Anti-mouse biotinylated antibody and streptavidin Cy3 fragment were used to detect PDI (**b**, **c**, **e**, **f**) or hs ALDP (**h**, **i**). (**a**) pBgm:EGFP, (**b**) anti-PDI staining of the same cell, (**c**) overlay of both pictures, (**d**) pEGFP:Bgm, (**e**) anti-PDI staining of the same cell, (**f**) overlay of both pictures, (**g**) pBgm:EGFP, (**h**) anti-hs ALDP staining of the same cell, and (**i**) overlay of both pictures. White size bars correspond to 50 μm.

Table 1 Fatty acid activation in cell extracts from COS-7 cells expressing EGFP–Bgm fusion proteins

COS-7 cells expressing pEGFP:Bgm or pEGFP-N1 vector alone were fractionated by differential centrifugation of homogenates. The results are expressed as the means ± S.D. for three independent experiments.

	Activty (nmol · 20 min^{-1} · mg of protein^{-1})		
Fatty acid substrate ...	$C_{16:0}$	$C_{18:2}$	$C_{24:0}$
Microsomal fraction			
pEGFP-N1	85.0 ± 6.7	91.9 ± 5.8	2.5 ± 0.2
pEGFP:mmBG	124.7 ± 9.9*	107.1 ± 10.2	4.0 ± 0.5*
Cytosolic fraction			
pEGFP-N1	3.4 ± 0.5	6.1 ± 1.3	0.1 ± 0.1
pEGFP:mmBG	7.1 ± 2.3	10.3 ± 2.1*	0.4 ± 0.3
Mitochondrial fraction†			
pEGFP-N1	20.4 ± 3.5	24.0 ± 7.6	0.8 ± 0.3
pEGFP:mmBG	23.8 ± 7.2	34.7 ± 5.3*	1.85 ± 0.9

* $P < 0.05$.
† Independent experiment.

in the cytosolic fraction. The purity of the microsomal fraction is illustrated by the fact that the peroxisomal ALDP could be detected exclusively within this light particle fraction. However, some of the fusion proteins are evident in the mitochondrial fraction (Figure 5A, lane 4). This could be due to a possible localization of the fusion protein within a cellular compartment termed mitochondrial-associated membrane, described by Rusinol et al. [42], since no distinct mitochondrial localization could be observed in confocal microscopy (Figure 6). Localization of the fusion proteins within the cytoplasmic fraction is considered to originate not from a distinct targeting of the proteins, but to result from experimental circumstances, such as misguiding of the fusion protein owing to its hydrophilic EGFP-domain or by destruction of cellular compartments during the fractionation procedure.

Further evidence for the localization of the mouse Bgm fusion constructs in microsomes is from the observation that the largest increase in ACS activity of Bgm-transfected cells resides in this fraction (Table 1). Besides, mitochondrial and cytosolic fractions showed a slight increase in activtity, especially towards linoleic acid, which is consistent with the finding of some protein in these fractions (Figure 5A, lanes 4 and 5). Analysis of the activation of different fatty acid substrates shows that Bgm has its highest activity for the LCFA $C_{16:0}$ (Table 1). However, the Bgm fusion protein was also capable of significantly activating lignoceric acid ($C_{24:0}$) to its acyl-CoA derivative (Table 1). In addition, a polyunsaturated LCFA, linoleic acid ($C_{18:2n-6}$), could be used as a substrate for esterification. Linoleic acid is the predominant

plant-derived polyunsaturated LCFA and is a precursor for arachidonic acid ($C_{20:4n-6}$) and eicosanoids [39], implying that Bgm plays a role in the anabolism of these molecules. Also, for the rat orthologue, activation of arachidonic acid and eicosapentanoic acid ($C_{20:5n-6}$) was clearly demonstrated [15]. Interestingly, the mitochondrial and cytoplasmic fractions showed a significant increase in linoleic acid activation. As reviewed by Coleman et al. [41], ACS exhibits different substrate specificities depending on their localization within the cell. This could be a possible explanation for our observation that the fusion protein seems to be targeted to two major compartments, the microsomal and mitochondrial, possibly mitochondrial-associated membrane, similar to that described for ACS4 [35]. For the cytoplasmic localization of the protein, we argue that the protein found in this fraction originates from either mistargeting or impurity of this fraction by preparation artifacts, similar to the presence of the EGFP protein in the mitochondrial fraction (Figure 5A, lane 1). This explanation is confirmed by the fact that confocal microscopy analysis localizes our fusion proteins exclusively to microsomal-like structures within the cell (Figures 6a, 6d and 6g). Results of the present study for the mouse Bgm protein are in good agreement with the observations made on the human Bgm orthologue [13]. In contrast with our findings, in the initial report of the mouse *Bgm* gene [14], the authors were not able to detect activity for VLCFA. Also the results presented on the rat Bgm orthologue revealed no activity on VLCFA but activity on polyunsaturated fatty acid was quite high [15]. Owing to the high similarity of mouse, human and rat genes a similar substrate specificity seems probable. Generally, all three proteins exhibit activity on LCFA, but in the previous studies only the human protein was capable of activating VLCFA. This discrepancy could be due to the fact that different fatty acid activity assays were used in these studies.

Results from the subcellular localization analyses confirm the computer predictions of the protein structure, which detected a single membrane-spanning domain in the N-terminal third of the protein. In addition, a putative peroxisomal PTS-2 localization signal and two putative ER retention signals could guide the protein to microsomal compartments. We also used confocal microscopy to investigate whether our Bgm fusion proteins co-localize with ER or peroxisomal proteins, as they were detected in the same fractions by Western-blot analysis (Figure 5). Both fusion constructs showed a clear punctated staining within the cell (Figures 6a, 6d and 6g). However, the signal did not co-localize with any of the markers we used for the subcellular localization experiments (Figures 6c, 6f and 6i). These observations suggest that the Bgm proteins are localized to microsomal structures within the cell, although we were not able to discriminate a distinct compartment. Taken together, these results show that the mouse Bgm protein is an ACS which resides mainly in microsomes and/or microsomal-like structures and is capable of activating VLCFA.

A VLC–acyl-CoA synthetase has long been suspected to play a putative role in X-ALD [12,40], but no enzyme with this activity showed the appropriate tissue distribution. The expression profile of Bgm, being enriched in brain, adrenals and testis, the target tissues of X-ALD, prompted us to investigate further the abundance of its mRNA during brain development. However, the temporal expression of the Bgm mRNA increases postnatally (Figure 3C) and thus differs from the Ald mRNA, which is detectable at midgestation of mouse embryonic development and decreases during postnatal development [26]. The distinctly different expression profiles during mouse brain development indicate that these two proteins act independently of each other. This observation is strengthened further by the fact that ALDP and the Bgm fusion protein do not show substantial subcellular co-localization (Figure 6i). In addition, we could not observe any difference in the amount of Bgm mRNA present in the brain of wild-type and Ald knockout mice (Figure 4). The lack of co-ordinated regulation and co-localization suggest that in the mouse the Ald and Bgm proteins are not functionally related. Thus the results do not support the model that was based on the *Drosophila* Bgm phenotype, implicating Bgm in fatty acid-related pathogenesis of X-ALD [12]. A phenotype comparable with the one seen in *Drosophila* [12] seems unlikely in a mammalian knockout of the *Bgm* gene. Further studies revealing the precise localization of the bubblegum protein and its distinct function within the cell will be needed to establish its role in fatty acid metabolism.

This work was funded by the Austrian Science Foundation (FWF grant no. P14163-MOB). We thank Professor W. Sieghart for providing the anti-EGFP antibody, M. Kunze for helpful discussions and F. Aboul-Enein for assistance with the confocal microscopy.

REFERENCES

1 Moser, H. W., Smith, K. D., Watkins, P. A., Powers, J. and Moser, A. B. (2000) X-linked adrenoleukodystrophy. In The Metabolic and Molecular Bases of Inherited Disease, 8th edn., vol. III (Scriver, C. R., Sly, W. S., Childs, B., Beaudet, A. L., Valle, D., Kinzler, K. W. and Vogelstein, B., eds.), pp. 3257–3301, McGraw-Hill, New York

2 Smith, K. D., Kemp, S., Braiterman, L. T., Lu, J.-F., Wei, H.-M., Geraghty, M., Stetten, G., Bergin, J. S., Pevsner, J. and Watkins, P. A. (1999) X-linked adrenoleukodystrophy: genes, mutations, and phenotypes. Neurochem. Res. **24**, 521–535

3 Roerig, P., Mayerhofer, P., Holzinger, A. and Gärtner, J. (2001) Characterization and functional analysis of the nucleotide binding fold in human peroxisomal ATP binding cassette transporters. FEBS Lett. **492**, 66–72

4 Tanaka, A. R., Tanabe, K., Morita, M., Kurisu, M., Kasiwayama, Y., Matsuo, M., Kioka, N., Amachi, T., Imanaka, T. and Ueda, K. (2002) ATP binding/hydrolysis by and phosphorylation of peroxisomal ATP-binding cassette proteins PMP70 (ABCD3) and adrenoleukodystrophy protein (ABCD1). J. Biol. Chem. **277**, 40142–40147

5 Lazo, O., Contreras, M., Hashmi, M., Stanley, W., Irazu, C. and Singh, I. (1988) Peroxisomal lignoceroyl-CoA ligase deficiency in childhood adrenoleukodystrophy and adrenomyeloneuropathy. Proc. Natl. Acad. Sci. U.S.A. **85**, 7647–7651

6 Uchiyama, A., Aoyama, T., Kamijo, K., Uchida, Y., Kondo, N., Orii, T. and Hashimoto, T. (1996) Molecular cloning of cDNA encoding rat very long-chain acyl-CoA synthetase. J. Biol. Chem. **271**, 30360–30365

7 Watkins, P. A., Lu, J. F., Steinberg, S. J., Gould, S. J., Smith, K. D. and Braiterman, L. T. (1998) Disruption of the *Saccharomyces cerevisiae* FAT1 gene decreases very long-chain fatty acyl-CoA synthetase activity and elevates intracellular very long-chain fatty acid concentrations. J. Biol. Chem. **273**, 18210–18219

8 Berger, J., Truppe, C., Neumann, H. and Forss-Petter, S. (1998) cDNA cloning and mRNA distribution of a mouse very long-chain acyl-CoA synthetase. FEBS Lett. **425**, 305–309

9 Berger, J., Truppe, C., Neumann, H. and Forss-Petter, S. (1998) A novel relative of the very long-chain acyl-CoA synthetase and fatty acid transporter protein genes with a distinct expression pattern. Biochem. Biophys. Res. Commun. **247**, 255–260

10 Heinzer, A. K., Kemp, S., Lu, J. F., Watkins, P. A. and Smith, K. D. (2002) Mouse very long-chain acyl-CoA synthetase in X-linked adrenoleukodystrophy. J. Biol. Chem. **277**, 28765–28773

11 Mihalik, S. J., Steinberg, S. J., Pei, Z., Park, J., Kim, do. G., Heinzer, A. K., Dacremont, G., Wanders, R. J., Cuebas, D. A., Smith, K. D. et al. (2002) Participation of two members of the very long-chain acyl-CoA synthetase family in bile acid synthesis and recycling. J. Biol. Chem. **277**, 24771–24779

12 Min, K.-T. and Benzer, S. (1999) Preventing neurodegeneration in the *Drosophila* mutant bubblegum. Science **284**, 1985–1988

13 Steinberg, S. J., Morgenthaler, J., Heinzer, A. K., Smith, K. D. and Watkins, P. A. (2000) Very long-chain acyl-CoA synthetases. Human 'bubblegum' represents a new family of proteins capable of activating very long-chain fatty acids. J. Biol. Chem. **275**, 35162–35169

14 Moriya-Sato, A., Hida, A., Inagawa-Ogashiwa, M., Wada, M. R., Sugiyama, K., Shimizu, J., Yabuki, T., Seyama, Y. and Hashimoto, N. (2000) Novel acyl-CoA synthetase in adrenoleukodystrophy target tissues. Biochem. Biophys. Res. Commun. **279**, 62–68

15 Tang, P. Z., Tsai-Morris, C. H. and Dufau, M. L. (2001) Cloning and characterisation of a hormonally regulated rat long chain acyl-CoA synthetase. Proc. Natl. Acad. Sci. U.S.A. **98**, 6581–6586

16 Forss-Petter, S., Werner, H., Berger, J., Lassmann, H., Molzer, B., Schwab, M. H., Bernheimer, H., Zimmermann, F. and Nave, K. A. (1997) Targeted inactivation of the X-linked adrenoleukodystrophy gene in mice. J. Neurosci. Res. **50**, 829–843
17 Boguski, M. S., Lowe, T. M. and Tolstoshev, C. M. (1993) dbEST – database for 'expressed sequence tags'. Nat. Genet. **4**, 332–333
18 Thomas, P. S. (1980) Hybridization of denatured RNA and small DNA fragments transferred to nitrocellulose. Proc. Natl. Acad. Sci. U.S.A. **77**, 5201–5205
19 Hasel, K. W. and Sutcliffe, J. G. (1990) Nucleotide sequence of a cDNA coding for mouse cyclophilin. Nucleic Acids Res. **18**, 4019
20 Danielson, P. E., Forss-Petter, S., Brow, M. A., Calavetta, L., Douglass, J., Milner, R. J. and Sutcliffe, J. G. (1988) p1B15: a cDNA clone of the rat mRNA encoding cyclophilin. DNA **7**, 261–267
21 Bradford, M. M. (1976) A rapid and sensitive method for the quantitation of microgram quantities of protein utilizing the principle of protein–dye binding. Anal. Biochem. **72**, 248–254
22 Steinberg, S. J., Wang, S. J., Kim, do. G., Mihalik, S. J. and Watkins, P. A. (1999) Human very long-chain acyl-CoA synthetase: cloning, topography, and relevance to branched-chain fatty acid metabolism. Biochem. Biophys. Res. Commun. **257**, 615–621
23 Ghilardi, N., Wiestner, A. and Skoda, R. C. (1998) Thrombopoietin production is inhibited by a translational mechanism. Blood **92**, 4023–4030
24 Morris, D. R. and Geballe, A. P. (2000) Upstream open reading frames as regulators of mRNA translation. Mol. Cell. Biol. **20**, 8635–8642
25 Xu, G., Rabadan-Diehl, C., Nikodemova, M., Wynn, P., Spiess, J. and Aguilera, G. (2001) Inhibition of corticotropin releasing hormone type-1 receptor translation by an upstream AUG triplet in the 5′ untranslated region. Mol. Pharmacol. **59**, 485–492
26 Berger, J., Albet, S., Bentejac, M., Netik, A., Holzinger, A., Roscher, A. A., Bugaut, M. and Forss-Petter, S. (1999) The four murine peroxisomal ABC-transporter genes differ in constitutive, inducible and developmental expression. Eur. J. Biochem. **265**, 719–727
27 Legakis, J. E. and Terlecky, S. R. (2001) PTS2 protein import into mammalian peroxisomes. Traffic **2**, 252–260
28 Inouye, S. and Tsuji, F. I. (1994) Aequorea green fluorescent protein. Expression of the gene and fluorescence characteristics of the recombinant protein. FEBS Lett. **341**, 277–280
29 Laitusis, A. L., Brostrom, M. A. and Brostrom, C. O. (1999) The dynamic role of GRP78/BiP in the coordination of mRNA translation with protein processing. J. Biol. Chem. **274**, 486–493
30 Muresan, Z. and Arvan, P. (1997) Thyroglobulin transport along the secretory pathway. Investigation of the role of molecular chaperone, GRP94, in protein export from the endoplasmic reticulum. J. Biol. Chem. **272**, 26095–26102
30a Erratum (1997) J. Biol. Chem. **272**, 30590
31 Mosser, J., Lutz, Y., Stoeckel, M. E., Sarde, C. O., Kretz, C., Douar, A. M., Lopez, J., Aubourg, P. and Mandel, J. L. (1994) The gene responsible for adrenoleukodystrophy encodes a peroxisomal membrane protein. Hum. Mol. Genet. **3**, 265–271
32 Mehtani, S., Gong, Q., Panella, J., Subbiah, S., Peffley, D. M. and Frankfater, A. (1998) *In vivo* expression of an alternatively spliced human tumor message that encodes a truncated form of cathepsin B. Subcellular distribution of the truncated enzyme in COS cells. J. Biol. Chem. **273**, 13236–13244
33 Shenkman, M., Ayalon, M. and Lederkremer, G. Z. (1997) Endoplasmic reticulum quality control of asialoglycoprotein receptor H2a involves a determinant for retention and not retrieval. Proc. Natl. Acad. Sci. U.S.A. **94**, 11363–11368
34 Lewin, T. M., Kim, J. H., Granger, D. A., Vance, J. E. and Coleman, R. A. (2001) Acyl-CoA synthetase isoforms 1, 4, and 5 are present in different subcellular membranes in rat liver and can be inhibited independently. J. Biol. Chem. **276**, 24674–24679
35 Lewin, T. M., Van Horn, C. G., Krisans, S. K. and Coleman, R. A. (2002) Rat liver acyl-CoA synthetase 4 is a peripheral-membrane protein located in two distinct subcellular organelles, peroxisomes, and mitochondrial-associated membrane. Arch. Biochem. Biophys. **404**, 263–270
36 Sakuma, S., Fujimoto, Y., Katoh, Y., Kitao, A. and Fujita, T. (2000) The regulation of prostaglandin and arachidonoyl-CoA formation from arachidonic acid in rabbit kidney medulla microsomes by palmitoyl-CoA. Life Sci. **66**, 1147–1153
37 Black, P. N., Zhang, Q., Weimar, J. D. and DiRusso, C. C. (1997) Mutational analysis of a fatty acyl-coenzyme A synthetase signature motif identifies seven amino acid residues that modulate fatty acid substrate specificity. J. Biol. Chem. **272**, 4896–4903
38 Black, P. N., DiRusso, C. C., Sherin, D., MacColl, R., Knudsen, J. and Weimar, J. D. (2000) Affinity labeling fatty acyl-CoA synthetase with 9-p-azidophenoxy nonanoic acid and the identification of the fatty acid-binding site. J. Biol. Chem. **275**, 38547–38553
39 Jump, D. B. (2002) The biochemistry of *n*-3 polyunsaturated fatty acids. J. Biol. Chem. **277**, 8755–8758
40 Barinaga, M. (1999) Mutant fruit flies respond to Lorenzo's oil. Science **284**, 1899–1901
41 Coleman, R. A., Lewin, T. M., Van Horn, C. G. and Gonzalez-Baro, M. R. (2002) Do long-chain acyl-CoA synthetases regulate fatty acid entry into synthetic versus degradative pathways? J. Nutr. **132**, 2123–2126
42 Rusinol, A. E., Cui, Z., Chen, M. H. and Vance, J. E. (1994) A unique mitochondria-associated membrane fraction from rat liver has a high capacity for lipid synthesis and contains pre-Golgi secretory proteins including nascent lipoproteins. J. Biol. Chem. **269**, 27494–27502

Received 16 July 2003/26 September 2003; accepted 30 September 2003
Published as BJ Immediate Publication 30 September 2003, DOI 10.1042/BJ20031062